Numerical And Experimental Investigation of The Flow Field Around NACA 0012 Aerofoil

[1]B. Raghava Rao, [2]Rangineni Sahitya

[1] Professor, Mechanical Department, VR Siddhartha Engineering College, Vijayawada,
[2] M.Tech Student, Mechanical Department, VR Siddhartha Engineering College, Vijayawada,

Abstract : In the present work, we studied experimental and numerical investigation of lift, drag coefficients and pressure distribution of two-dimensional subsonic stream over National Advisory Committee for Aeronautics NACA 0012 symmetric aerofoil at different angles of attack and at low and high Reynolds numbers (Re). The results are presented for every two degrees of angle of attack from -20^0 to 20^0 at velocity of 45m/s. The computational domain was made of 80000 elements for NACA 0012 in a structured manner, dealing with the refinement of the grid around the aerofoil keeping in mind the end goal is to enclose the boundary layer. The popular turbulent models for simulation are Spalart-Allmaras, K-Omega (Shear Stress Transport) is validated and examining the predictions of the free field experimental measurements in laminar flow for the aerofoils selected. The experimental test was conducted in low-speed wind tunnel, and the numerical analysis was performed using CFD program in ANSYS-15 (FLUENT) software. The main purpose of the work was to demonstrate the behavior of the aerofoil at these conditions and to build up a verified solution method. The simulated results acquired from numerical and experimental were compared which shows close agreement with the literature results. In this study, Stall angle relies on turbulent occurred behind aerofoil; therefore as a result impact of the stall angle performance was investigated.

Keywords: Aerofoil, Angle of attack, CFD, Fluent, Lift and Drag, NACA 0012, Turbulence models, Wind tunnel.

I. INTRODUCTION

The information useful for solving aerodynamic problems of Aeronautical, Space, Automobile and Civil Engineering structures, are best obtained rapidly , economically and accurately by testing the scaled models, and sometimes actual structure in Wind Tunnels . The size, speed and other environmental conditions of tunnel are determined by the actual users problems. Leaving the size and environmental to the actual users, the speed determines the type of the tunnel namely, subsonic (low speed), Transonic, Super-sonic and Hyper-sonic. While the speeds of these tunnels are obviously named with reference to the sonic velocity, the low speed subsonic tunnel which is of our concern is below 300 mph. An alternative definition to the low speed tunnel would be the tunnel where the compressibility of air is negligible.

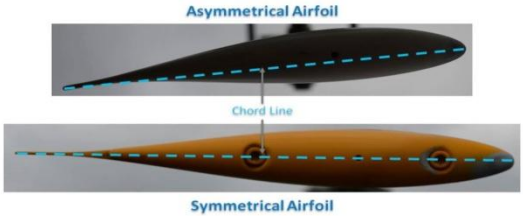

Fig. 1 Cross section of an symmetric and un- symmetric aerofoil

A wind tunnel examination enables determining the aerodynamic forces acting on a given structure. Such knowledge is particularly useful for calculating the strength of structures especially during high-speed winds. The main objectives of the present work is to determine the lift and drag forces on aerofoils. As shown in the Figure 1.2, the research assumes airflow or suction to proceed from the aerofoil top surface. Several types of aerofoils are tested in terms of different values of wind velocities and angles of attack.

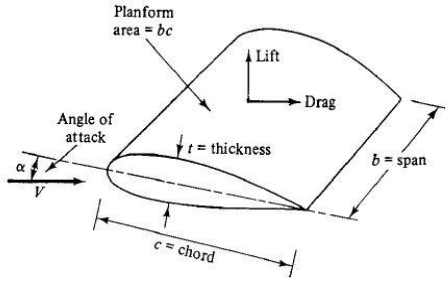

Fig. 2 Geometry and dynamic parameters of aerofoil

Experimental investigations are very important due to results. However, these take much time and uneconomic and whenever we want to change a parameter about our study, it is very difficult because of time and cost. Fortunately, investigators can study behaviour very fast numerical approach and thanks to computational fluid dynamics (CFD) programs. These programs can give as close results as experimental methods. Also, CFD programs can be contributed as regards time and faster compared to experimental methods. The rapid evolution of computational fluid dynamics (CFD) has been driven

by the need for faster and more accurate methods for the calculations of flow fields around configurations of technical interest. In the past decade, CFD was the method of choice in the design of many aerospace, automotive and industrial components and processes in which fluid or gas flows play a major role. When simulating the flow over aerofoils, transition from laminar to turbulent flow plays an important role in determining the flow features and in quantifying the aerofoil performance such as lift and drag. Hence, the proper modelling of transition, including both the onset and extent of transition will definitely lead to a more accurate drag prediction. The flow was obtained by solving the steady-state governing equations of continuity and momentum conservation combined with one of three turbulence models Spalart-Allmaras, Realizable K-Epsilon and K-Omega shear stress transport (SST) aiming to the validation of these models through the comparison of the predictions and the free field experimental measurements for the selected aerofoil.

II. EXPERIMENTAL SETUP

The experiments have been conducted in an low speed, open circuit wind tunnel at VR Siddhartha engineering college. This tunnel test section size is about 300mm × 300mm from the figure 2.1. The aerofoil used in the present study is NACA 0012 profile of chord length, C, of 0.1m and span wise length, S, of 0.295m. Stationary end plates are kept on the two sides of the aerofoil, with a small gap of about 1mm, to help maintain two dimensionality of the flow. The experiments have been conducted at 45m/s wind velocity (V) in tunnel which is corresponding to 3×10^5 Reynolds number (Re).

Fig. 3 Subsonic wind tunnel test area

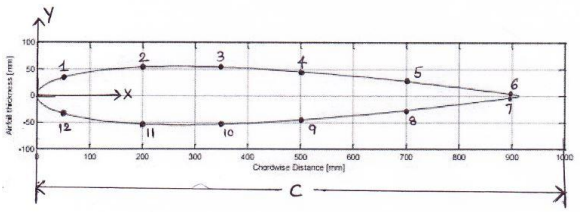

Fig. 4 Schematic of the aerofoil pressure tapping locations

(1) to (12) - Pressure tapping locations on the aerofoil

(13) - Tunnel wall static pressure

Other tubes - Open to atmosphere

Wind tunnel works on the idea that a stationary model with air moving around it behaves the same way a real, full scale airplane moving through stationary air does. Here we are using an aerofoil for testing. This is usually made out of steel or aluminum. The tunnel balance is three component type designed using electrical strain gauges to indicate separately on the digital indicator. The balance is intended for indicating the Lift, Drag, Side forces and this model is mounted on the string situated exactly beneath the test section. The output from the Lift, Drag, Side forces are connected to their respective multi-pin sockets provided at control panel.

Main parts:

Honeycomb inlet mesh screen, Effuser, Blower unit with AC motor and thyristor controller, Three component like Lift, Drag, Side force balances, Multi-tube manometer, Smoke generator constitute the complete tunnel.

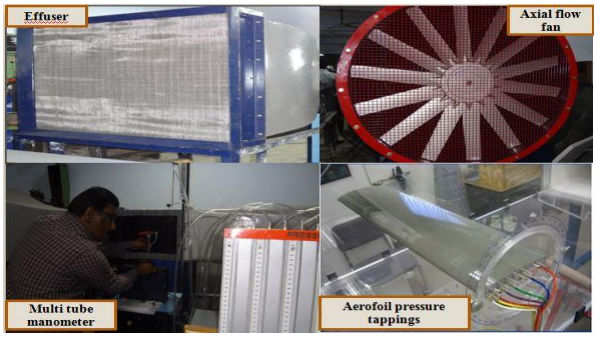

Fig. 5 Components of wind tunnel

A. Inlet duct (Effuser):

It is aerodynamically contoured section with contraction area ratio 9:1. The inlet starts with dimension of 900mm x 900mm contoured to 300mm x 300mm. The axial and lateral turbulence are reduced and smooth flow of air entering the section is achieved by installing the Honey-combs and screens, for most effectiveness of the air inlet. The ratio of length to cell size of the Honey-comb is maintained as per the recommended standards. The wire mesh is also fixed to smoothen the flow, further. This is particularly useful for obtaining laminar flow. The screen is made removable for possible cleaning. The duct is secured to the test section by flange. The provision is also made for easy removal of Effuser and diffuser for possible separation from the test section when required. It is also highly smoothened and painted.

B. Test section:

The central portion of the test section sandwiched between the inlet duct (Effuser) and the diffuser using flange. It has 300mm x 300mm cross section (inside) and 550mm length. Fixed with transparent window on either side which facilitates fixing and

viewing of the models. This houses smoke chest fixing points. The traversing mechanism is fixed on its top of the movement of total pressure probe .The holes provided for holding the models for different studies and for taping out the pressure probes.

C. Diffuser:

The downstream portion of the tunnel is the diffuser .To the end of this is attached an axial flow fan . The diffuser starts with 300mm x 300mm square section at the test section end and enlarges to 900mm diameter round at the fan driven end . It is flanged and bolted to the test section.

D. Axial flow fan unit:

The axial flow fan driven by AC motor (10Hp) with AC drive for speed controlling is independent stand alone type and does not require any foundation. It is housed in rounded casing which is secure to the diffuser. The bladed rotor is connected to AC motor directly coupled.

E: Multi tube manometer:

This is used for studying pressure distribution across various models, Viz., Aerofoil, cylinder, special purpose shapes. It contains 13 number of tubes mounted on board with adjustable inclination. Bottom of all tubes are interconnected and in turn to the balancing reservoir filled with colored water. While the last tube is left open to atmosphere for reference, all other 12 tubes are connected at their top to pipe tube bundles of the model. The required model is held in the test section between holes provided front and back side Perspex windows. The pressure tapings (tube outlets) are connected to the glass limbs of the respective Serial Number. The required degree of angle of inclination can be given to the tube bundle and angle measured with respect to the horizontal .

F. Control console:

The tunnel has two consoles, one for the air speed control (AC motor Controller) and the other for the indication of velocity head and forces. The console which houses tyhristor speed controller connected to AC motor by 3 ph, 440 V, AC supply. All safety precaution for excessive electrical loading are provided.

III. CFD METHODOLOGY

Computational Fluid Dynamics (CFD) is a numerical method used to simulate physical problems with use of governing equations. This method can be used to investigate design approaches without creating a physical model and can be a valuable tool to understand conceptual properties of new mechanical designs. By using a simulation instead of doing lab experiments, one may acquire results faster and with less expense. An important aspect in the use of CFD is to understand the simplifications in software, and know the limitations in the computed results. Though the CFD software uses well known governing equations, severe simplifications are made in terms of grid and representing geometries.

In this paper, the NACA 0012, the well documented aerofoil from the 4-digit series of NACA aerofoils are utilized. The NACA 0012 aerofoil is symmetrical, the 00 indicated that it has no camber. The 12 indicates that the aerofoil has a 12% thickness to chord length ratio. Reynolds number for the simulations was Re = 3×10^5, same with the experimental data from the above, in order to validate the present simulation.

Approach:

Following is the method employed to carry through the CFD simulation

1 Preparing geometric model

2 Generate meshing

3 Setting boundary conditions

4 Software (Fluent) setup, initialization and solving

4.1 Laminar model

4.2 Turbulent (Viscosity) model

1. Preparing geometric model

NACA 0012 symmetric aerofoil geometry was acquired as co-ordinate vertices i.e. texts file and imported into the ANSYS FLUENT. Some adjustments were made to this to correct the geometry and make it valid as a CFD model.

FLUENT is essential in the process of doing the CFD analysis, it creates the working environment where the object is simulated. An important part in this is creating the mesh surrounding the object. This needs to be extended in all directions to get the physical properties of the surrounding fluid in this case moving air. The mesh and edges must also be grouped in order to set the necessary boundary conditions effectively.

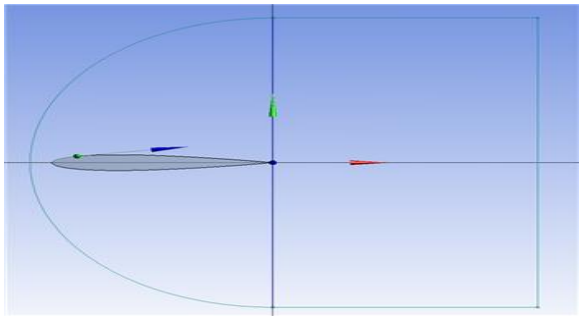

Fig. 6 Geometry model of aerofoil

Firstly we have to import the coordinates of aerofoil and create the curve, the 2D analysis type is used and launch the design model created. Then we need to create the surface to the curve then the aerofoil is generated. We need to create the meshing surface we will use once we begin to specify boundary conditions. We will begin by creating a coordinate system at the tail of the aerofoil this will help us create the geometry for the C-mesh domain by using sketcher toolbox and dimension tool

box. Next, we need to create a surface from this sketch. The final step of creating the C-Mesh is creating a surface between the boundary and the aerofoil by using Boolean operations. In the final step of creating the geometry, we will split up the new surface into 4 quadrants; this will be useful for meshing the geometry. The geometry is finished. Save the project and close the design modeler, as we are now we are ready to create the mesh for the simulation.

2. Generate meshing

An environment consisting of 2 squares and 1 semicircle surrounds the NACA 0012 symmetrical aerofoil. The mesh is constructed to be very fine at regions close to the aerofoil and with high energy, and coarser farther away from the aerofoil. For this aerofoil a structured quadratic mesh was used.

Due to limitations in the FLUENT software, the mesh has to be fine also in certain regions far from the aerofoil. A fine mesh implies a higher number of calculations which in turn makes the simulation use longer time to finish. For the NACA aerofoils, the grid distributed with an increasing distance between nodes, starting from very small sizes from the leading edge. From the point of max thickness on the aerofoil to the trailing edge an even number of points is distributed on the aerofoil surface.

Grid convergence: Two different meshes are made to the CFD simulations. This is to test the grid convergence, how the change in number of cells, and hence also cell size, affect the end result.

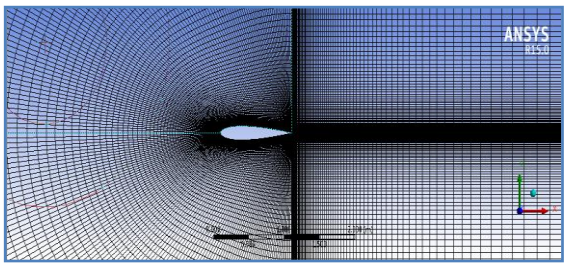

Fig. 7 Mesh around NACA 0012 aerofoil for 100 number of divisions

(80000 elements) for the CFD simulation

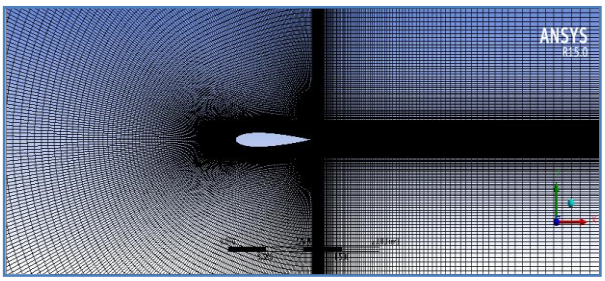

Fig. 8 Mesh around NACA 0012 aerofoil for 150 number of divisions

(100000 elements) for the CFD simulation

As per calculating the end results on the above different types of mesh ups at velocity 45m/s and 10^0 angle of attack as shown in table 3.1 below.

Table 1 Grid test

GRIDS(quad)	Lift coefficient (C_L)
5000	0.7134
10000	1.0036
20000	1.0716
40000	1.110
60000	1.127
80000	1.138
100000	1.138

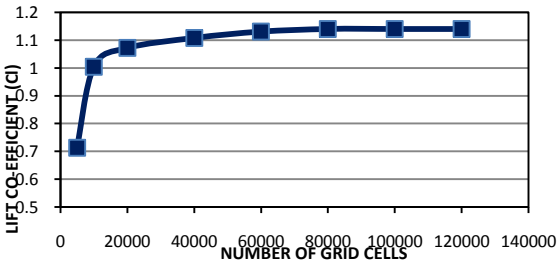

Fig. 9 Curve of lift coefficient (C_L) vs number of grid cells for symmetric aerofoil NACA 0012 at velocity V=45m/s and angle of attack $\alpha=10^0$

Lift coefficient is calculated at angle of attack 10^0. Comparison of the end results of different mesh sizes shows the minimum deviation of results with the quadrilateral meshing having number of elements 80000 as shown above in figure 3.4. After that mesh results are not so much affected by followed mesh ups so the all simulations are done on the same mesh file and validating the final results with experimental data.

3. Setting boundary conditions

Giving properties to the different geometries is vital to make the simulation work. In this case, the mesh boundaries were given set to the x and y velocity components, and the end boundary the property "pressure-outlet" to simulate the zero gauge pressure. The aerofoil itself is given as wall properties.

Table 2 Operating parameters

INPUT	VALUE
Velocity of flow	0.13 Mach or 45 m/s
Operating temperature	300 k
Operating pressure	101325 pa
Models	Inviscid K-Omega(SST) Spalart-Allmaras
Density of fluid	1.225 kg/m³
Kinematic viscosity	$1.4607 \times E^{-5}$ kg/ms
Angle of attack	0° to 20°
Fluid	Air

4. Setting up FLUENT (Initializing and solving)

The geometry and mesh were imported into FLUENT, and the system and environment properties set "PRESTO!" and "Double precision" is selected as system parameters, ensuring adequate accuracy. FLUENT has single precision as default, but for these simulations an accurate solution is requested. The residuals for the different turbulence model variables were set to $10e^{-6}$and the iteration max count to 1000. The simulation process could also be halted or stopped if the C_L or C_D seemed to have stabilized properly.

4.1. Laminar model

Laminar flow (streamline flow) occurs when a fluid flows in parallel layers, with no disruption between the layers at low velocities, the fluid tends to flow without lateral mixing, and adjacent layers slide past one another. Laminar flow occurs at low Reynolds numbers, where viscous forces are dominant, and is characterized by smooth, constant fluid motion. Consider the flow over an aerofoil. The boundary layer is a very thin sheet of air lying over the surface of the wing (and all other surfaces of the aerofoil). Because air has viscosity, this layer of air tends to adhere to the wing. As the wing moves forward through the air, the boundary layer at first flows smoothly over the streamlined shape of the aerofoil. Here, the flow is laminar and the boundary layer is a laminar layer. Laminar flow is a flow regime characterized by high momentum diffusion and low momentum convection.

4.2 Turbulent models

Considering vortex shedding and boundary layer separation for aerofoils and wings, this simulation will have to deal with turbulent flows. The chaotic nature of turbulent flow makes it very expensive to compute velocities for all points in space. RANS (Reynolds-Averaged Navier-Stokes) is the opposite to DNS (Direct Navier-Stoke) which is the analytic direct simulation of the governing equations, and use a statistical and averaged approach to find the flow behaviour. The reason for using RANS models is that small vortices in turn very expensive to solve are removed by averaging the flow.

A crucial point is selecting a viscous model, and in FLUENT there are several options. There are fundamental differences to the different models, and may be used for different types of flows. In this, the viscous models Realizable (k-ε) and Spalart-Allmaras and k-ω (Shear stress transport) are used. Realizable (k-ε) and k-ω (Shear stress transport) are 2-equation models, whilst Spalart-Allmaras (S-A) is a newer 1-equation model.

IV. RESULTS AND DISCUSSION

In this study, experimental and numerical analysis were performed. The experimental are conducted at 45m/s wind velocity. Lift, drag coefficient and pressure distribution of NACA 0012 aerofoil at different angles of attack between -20^0 and 20^0 are measured. Also the lift, drag coefficients and pressure distribution are obtained as numerical with FLUENT programs for the same conditions. The simulated results acquired from numerical and experimental methods were compared which shows close agreement with the literature results.

A. Experimental results:

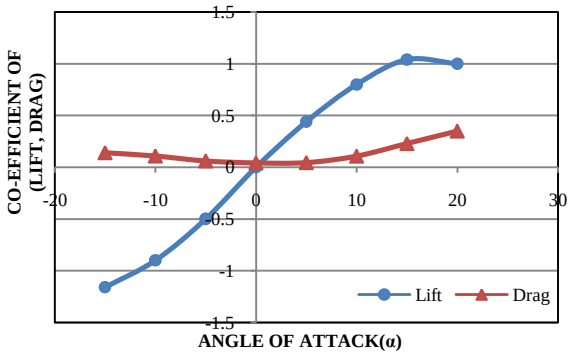

Fig. 10 Coefficient of lift (C_L), drag (C_D) forces vs angle of attack (α) on NACA 0012 aerofoil at velocity of 45m/s

The lift, drag coefficient for NACA 0012 airfoil are measured as experimentally. The maximum lift and drag coefficients were found as 1.04 and 0.35 for 15^0 angle of attack from figure 4.1. The lift and drag coefficient was primarily effected by angle of attack as regards both increasing and decreasing. If angle of attack increased, lift and drag coefficient could increase until certain angle. After certain angle, the lift coefficient was decreasing whereas; drag coefficient increased. This situation is called as stall angle. The stall angle caused transition from laminar to turbulence flow.

The pressure distribution of NACA 0012 at angles of attack ranging from -20^0 to 20^0 is observed.

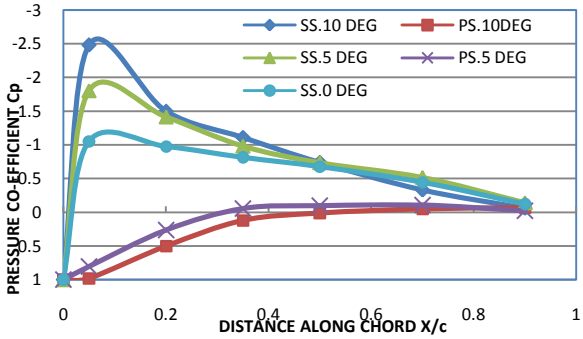

Fig. 11 Coefficient of lift (C_L), drag (C_D) forces vs angle of attack (α) on NACA 0012 aerofoil at velocity of 45m/s

From figure 4.2 for all angles of attack, the pressure coefficient had a large suction peak at the suction surface (SS) near the leading edge and followed by a gradual increase in pressure. The suction peak of the pressure side (PS) was obtained near the leading edge, where pressure coefficient attained maximum value. At $\alpha=0^0$, the pressure variation over the suction pressure side of aerofoil showed a symmetric distribution. Suction peaks of the suction side were in the range of -

1.2 and -2.5 from 0^0 to 10^0 angles of attack. A slight increase and then subsequent decrease was obtained in the C_p curves of suction surface. It can be said that from the curves that the boundary layer developed after peak suction from the leading edge to trailing edge the pressure slowly increased.

B. Simulated results:

Simulations for various angles of attack ranging from -20^0 to 20^0 at velocity 45m/s are done in order to compare the results from the different turbulent models, K-Omega (Shear Stress Transport) and Spalart-Allmaras and these are validated with existing literature results and also with the experimental results.

Contours of static pressure over NACA 0012 aerofoil

The contour results for different turbulent models are shown below for NACA 0012 symmetric aerofoil at velocity of 45m/s.

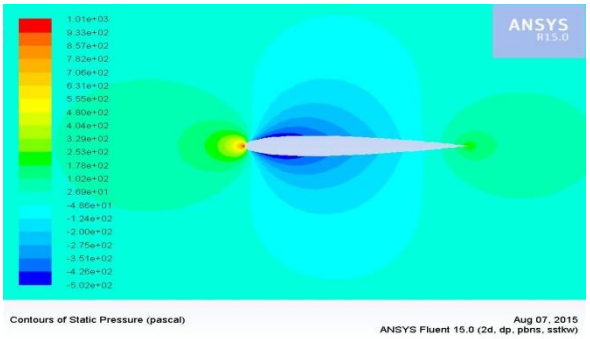

Fig. 12 Contours of static pressure at 0^0 angle of attack with K-Omega turbulent model

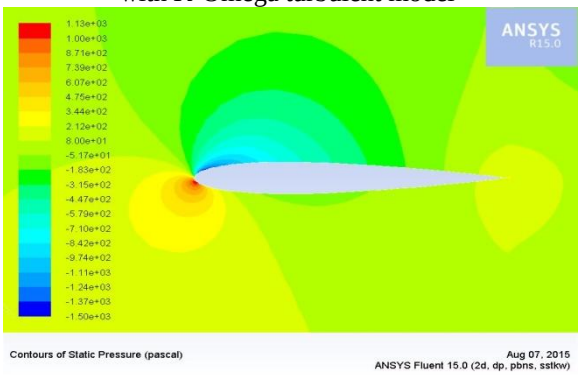

Fig. 13 Contours of static pressure at 4^0 angle of attack with K-Omega turbulent model

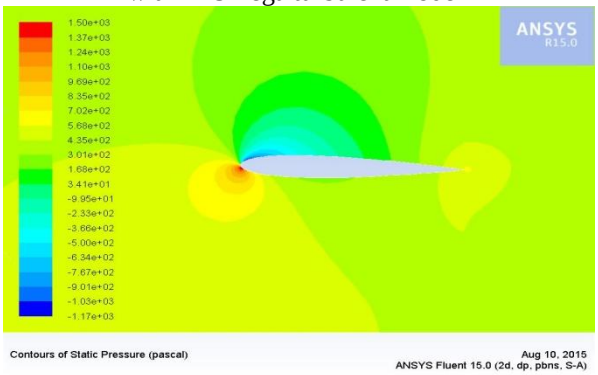

Fig. 14 Contours of static pressure at 4^0 angle of attack with Spalart-Allmaras turbulent model

From the contours of static pressure, we can see that there is a region of high pressure at the leading edge and region of low pressure on the upper surface of aerofoil. For 0^0 angle of attack from figure 4.3, we obtain that the contours of static pressure over an aerofoil is symmetrical for both upper and lower surfaces and stagnation point is exactly at the nose of an aerofoil. For 4^0 angle of attack, we see that the flow has a stagnation point just under the leading edge and hence producing lift as there is a low pressure region on the upper surface of the aerofoil as shown in figure 4.5. By comparing these two turbulent models the K-Omega model results have more static pressure output when compared to Spalart-Allmaras model.

Contours of velocity magnitude over NACA 0012 aerofoil

The contour results for different turbulent models are shown below for NACA 0012 symmetric aerofoil at velocity of 45m/s.

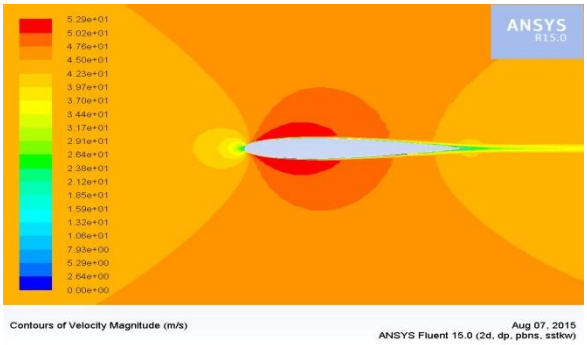

Fig. 15 Contours of velocity magnitude at 0^0 angle of attack with K-Omega turbulent model

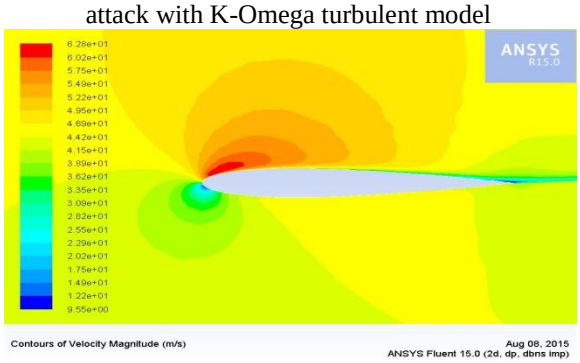

Fig. 16 Contours of velocity magnitude at 4^0 angle of attack with K-Omega turbulent model

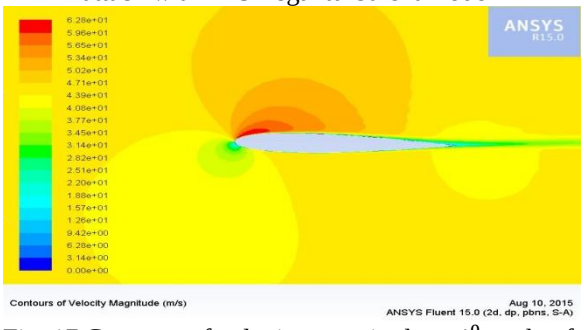

Fig. 17 Contours of velocity magnitude at 4^0 angle of attack with Spalart-Allmaras turbulent model

From the contours of velocity magnitude, we see that the upper surface of the aerofoil experienced a high velocity compared to lower surface. As the angle of attack increases the velocity at upper surface was much higher than the velocity at lower surface. On the leading edge, we see a stagnation point where the velocity of the flow is nearly zero. The fluid accelerates on the upper surface decelerates and converges with the flow on the lower surface. For 0^0 angle of attack from figure 4.6 the velocity contours are same as symmetrical and from figure 4.8 at 4^0 angle of attack the stagnation point is slightly shift towards the trailing edge via bottom surface, hence it will create low velocity region at the lower side of the aerofoil and high velocity at the upper side of the aerofoil.

Hence coefficient of lift will increase and coefficient of drag will also increase but increasing in drag is low compare to increasing in lift force. By comparing these two turbulent models the K-Omega model results have more velocity magnitude output when compared to Spalart-Allmaras model.

Curves of pressure coefficients

The pressure distribution of the NACA 0012 aerofoil at -20^0 to 20^0 angles of attack are shown in figures 4.9 and 4.10. The simulations are done for two turbulent models, K-Omega and Spalart-Allmaras models.

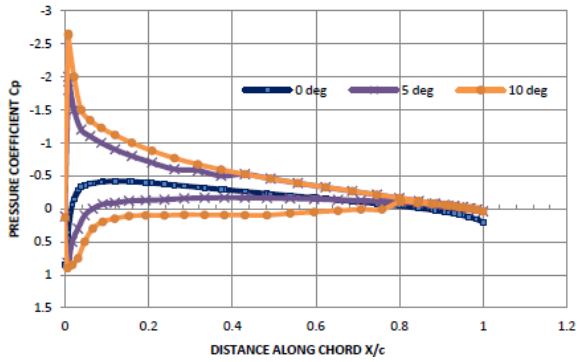

Fig. 18 Variation of surface pressure Coefficients (C_P) on NACA 0012 aerofoil for turbulent K-Omega flow at different angles of attack at 45m/s

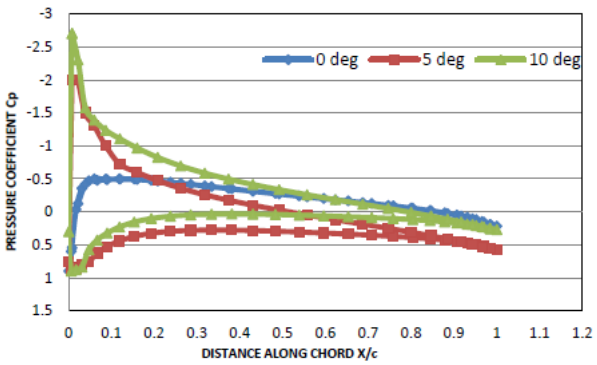

Fig. 19 Variation of surface pressure Coefficients (C_P) on NACA 0012 aerofoil for turbulent Spalart-Allmaras flow at different angles of attack at 45m/s

From figure 4.9 and 4.10 for all angles of attack, the pressure coefficient had a large suction peak at the suction surface (SS) near the leading edge and followed by a gradual increase in pressure. The suction peak of the pressure side (PS) was obtained near the leading edge, where pressure coefficient attained maximum value. At $\alpha=0^0$, the pressure variation over the suction pressure side of aerofoil showed a symmetric distribution. Suction peaks of the suction side were in the range of -1.2 and -2.6 for K-Omega model and -1.5 to -2.7 for Spalart-Allmaras from 0^0 to 10^0 angles of attack. A slight increase and then subsequent decrease was obtained in the C_P curves of suction surface in fig 4.9 and 4.10. It can be said that from the curves that the boundary layer developed after peak suction from the leading edge to trailing edge the pressure slowly increased. By comparing these two turbulent models the K-Omega model results have more coefficient of pressure output when compared to Spalart-Allmaras.

Curves of lift and drag coefficients

The curves of lift and drag coefficients are computed at various angles of attack using two turbulent models, Spalart-Allmaras and K-Omega model. These two methods are compared with experimental results and validated with existing literature results for NACA 0012 aerofoil, yields a good correlation for lift slope and stall angle.

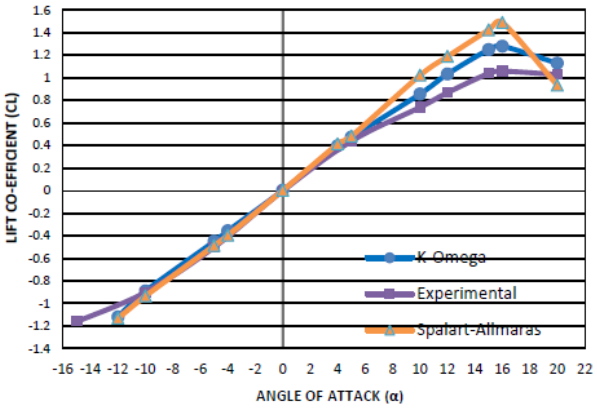

Fig. 20 Comparison between experimental data and two turbulent models simulation results of the lift coefficient curve for NACA 0012 aerofoil at velocity of 45m/s

The figure 4.11 shows that at low angles of attack, the dimensionless lift coefficient increased linearly with increasing angles of attack. At an angle of attack of roughly 15^0 to 16^0, the flow on the upper surface of the aerofoil began to separate and this condition is known as stall angle. These two models had a good agreement with the experimental data at angles of attack from -20^0 to 20^0 and the same behavior at all angles of attack until stall. K-Omega method showed similarity with the experimental results as shown in figure 4.11. The best results of lift and drag were obtained at 16^0 angle of attack.

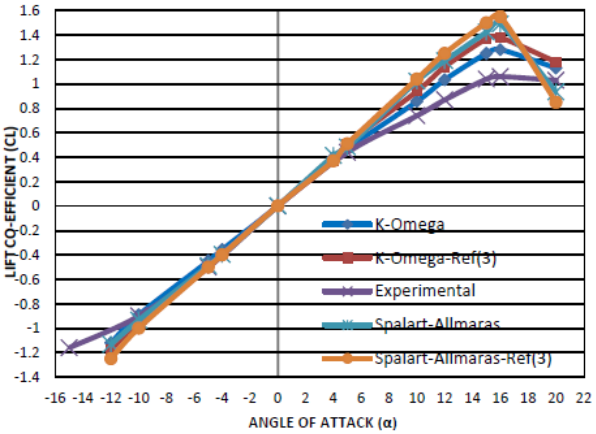

Fig. 21 Comparison between experimental data and two turbulent models simulation results with literature results of the lift coefficient curve for NACA 0012 aerofoil at velocity of 45m/s

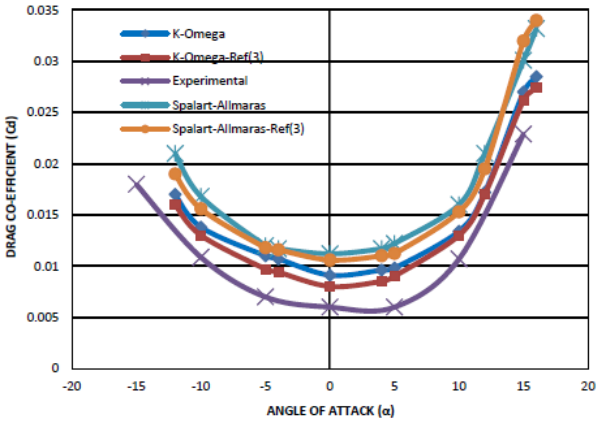

Fig. 22 Comparison between experimental data and two turbulent models simulation results with literature results of the drag coefficient curve for NACA 0012 aerofoil at velocity of 45m/s

From the literature results from reference (3) the comparison between experimental data and two turbulent models simulated results for lift and drag coefficients are observed. The lift coefficient increases and drag coefficient increases as stall increases. Near stall disagreement between the data was shown. The predicted drag coefficients are higher than the experimental data as shown in figure 4.13. This over prediction of drag is expected since the actual aerofoil has laminar flow over the forward half. The turbulence models cannot calculate the transition point laminar to turbulent and consider that the boundary layer is turbulent throughout its length. The values of drag coefficient from the turbulent models are compared to experimental data. The most accurate model is K-Omega SST model when compared to Spalart-Allmaras model for both lift and drag coefficients.

V. CONCLUSIONS

In the present work aerodynamic characteristics have been evaluated for symmetric NACA 0012 aerofoil. In this context, comparison between pressure coefficients and force coefficients at different angle of attacks have been studied. Simulations are done on the different mesh ups and turbulent models at velocity of 45m/s. These simulations provide best approachable results to experimental data for laminar and turbulent models.

The simulations for various angles of attack were done in order to be able to compare the results from the different turbulence models and experimental results and validate them with existing literature data from reliable sources. To do so, the model was solved with a range of different angles of attack from -12 to 20°. At low angles of attack, the dimensionless lift coefficient increased linearly with angle of attack. Flow was attached to the aerofoil throughout this regime. At an angle of attack of roughly 15 to 16°, the flow on the upper surface of the aerofoil began to separate and a condition known as stall began to develop and the same behavior at all angles of attack until stall. It was obvious that the K-Omega turbulence model had the same behavior with the experimental data as well as after stall angle. The most appropriate turbulence model for these simulations was the K-Omega (SST) two-equation model when compared to Spalart-Allmaras one-equation model.

The other designed NACA 0015 symmetrical aerofoil and NACA 4412 un-symmetrical aerofoil are also investigated and simulated at same angles of attack ranging from -20^0 to 20^0 and at different velocities ranging from 10m/s to 50m/s. And these models are also validated with the literature results from different sources, which showed close agreement with the results compared. This paper shows validation for only one model NACA 0012 symmetrical aerofoil, hence it is concluded that the modeling and simulated results which are validated by keeping in mind the end goal is to choose the appropriate model for simulation.

REFERENCES

[1] İzzet Şahin and Adem Acir, 2015, "Numerical and Experimental Investigations of Lift and Drag Performances of NACA 0015 Wind Turbine aerofoil". International Journal of Materials, Mechanics and Manufacturing, Vol. 3, No.1, pp 22-25.

[2] Amit Kumar Saraf; Man Vijay Singh; Ajay Kumar, International Journal of Scientific and Engineering Research, Volume 3, Issue 8, August-2012 1 ISSN 2229-5518 Page No. 001-007.

[3] Douvi C. Eleni*, Tsavalos I. Athanasios and Margaris P. Dionissios Evaluation of the turbulence models for the simulation of the flow over a National Advisory Committee for Aeronautics (NACA) 0012 aerofoil ,JMER vol 4(3)pp100-111March(2012).

[4] Abbott IH, Von Doenhoff AE. Theory of Wing Sections. ISBN 486-60586 8Dover\Publishing, New York. (1959).

[5] Dr. J. M. Meyers | Dr. D. G. Fletcher | Dr. Y. Dubief, Lift and Drag on an Airfoil, ME 123: Mechanical Engineering Laboratory II: Fluids, 2008.

[6] Miller, S. D., "Wind Tunnels". Aerospace Engineering, The Ohio State University, Columbus, 2008.

[7] Haritonidis, J. H., "Lift, Drag and Moment of a NACA 0015 Aerofoil". Aerospace Engineering, The Ohio State University, Columbus, 2008.

[8] Onur Yemenici, "Experimental Investigation of the Flow Field Around, NACA0012 Airfoil", Vol 2 – Aug-2013